THE JOURNAL OF PHYSICAL CHEMISTRY C
A JOURNAL OF THE AMERICAN CHEMICAL SOCIETY



pubs.acs.org/JPCC
Article

# Nanoscale Morphology of the PTCDI-C13/PMMA Interface: An Integrated Molecular Dynamics and Atomic Force Microscopy Approach

Andrea Lorenzoni, Federico Prescimone, Marco Brucale, Stefano Toffanin, and Francesco Mercuri*

Cite This: *J. Phys. Chem. C* 2023, 127, 18026−18035



**ABSTRACT:** The morphology of molecular aggregates at interfaces impacts strongly on the functional properties of nanoscale systems for electronic and optoelectronic applications. The packing of organic materials on surfaces, in turn, depends on several factors, including the nature and structure of the substrate, the fabrication conditions, and processing. In this work, we perform an integrated computational/experimental study to unravel the details of the molecular aggregation morphology at the interface between two organic materials. Namely, we address the morphology of aggregates of *N*,*N*′-ditridecylperylene-3,4,9,10-tetracarboxylic diimide (PTCDI-C13), a prototypical n-type organic semiconductor at the interface with poly-methyl metacrylate (PMMA), an organic polymer commonly used as a dielectric layer in devices. The integration between molecular dynamics simulations and atomic force microscopy experiments elucidates the critical role of growth and post-processing conditions in the formation of the interface structure.

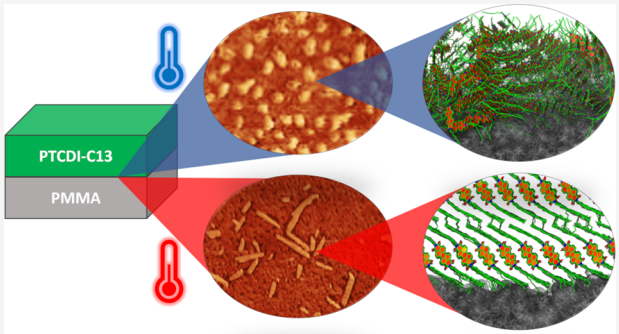


## ■ INTRODUCTION

The development of organic electronic devices is strongly connected to the properties of functional organic molecular materials, thin films, and interfaces.[1−6] In turn, the properties of organic materials are often related to intermolecular aggregation phenomena and to the nanoscale morphology of organic layers.[7−13] In molecular systems, aggregation is induced essentially by weak van der Waals interactions, which result in different possible aggregation structures with relatively small energy differences and low interconversion barriers from each other.[8] The aggregation of small molecules at the solid state leads usually to different possible packing structures and aggregation morphologies, also manifested as bulk polymorphism, as a function of growth and fabrication conditions.[14−20] The occurrence of different structural motifs in molecular aggregates also affects the morphology of molecular thin-films at the interface with substrates, which is of paramount relevance in the development of technological applications in organic electronics and bioelectronics.[11,12,19,21−25] In thin-films of organic materials, molecular aggregation is also related to the interaction of the molecular layer with the supporting substrate.[10,18,22,26−30] Details related to fabrication conditions and processing also play a significant role in determining the morphology of organic thin-films.[22,28,31−34] The morphology of molecular aggregates at the interface with a substrate depends, therefore, on a broad set of variables, from molecular structure to properties of the substrate (materials, microscopic, and mesoscopic morphology), fabrication conditions, processing, and thickness of the organic layer.[35] The details of the morphology of organic molecular materials' impact on their functional properties are used to develop devices such as organic light-emitting diodes, field-effect, electrochemical, and light-emitting transistors or photovoltaic cells. Namely, molecular packing influences strongly the transport of charge carriers (including charge and exciton diffusion and recombination) in organic semiconducting layers, with a significant impact on the performance of devices.[11,32,33,36−43] Understanding the relationship between molecular structure of organic active materials, processing methodologies and architectures, and resulting functional properties is, therefore, one of the main research targets for the development of organic electronics.[44,45]

In the past few years, significant research efforts have been targeted toward this issue. Particularly, recent work has demonstrated the potential of joint experimental/computational endeavors for unraveling the relationship between the chemical structure of organic molecules and the resulting properties in complex aggregates and at interfaces.[46−49] These

**Received:** May 18, 2023
**Revised:** July 25, 2023
**Published:** September 6, 2023







https://doi.org/10.1021/acs.jpcc.3c03332
*J. Phys. Chem. C* 2023, 127, 18026−18035

studies demonstrated that the structural variability of molecular aggregates at interfaces requires detailed investigations on the microscopic nature of the different aggregation morphologies as a function of fabrication conditions, processing, thickness, and other fabrication variables.

In this work, we perform computational studies and experimental validations to assess the nanoscale aggregation in thin-films of a well-assessed and multifunctional semiconducting n-type organic small-molecule, namely the perylene diimide derivative *N*,*N*′-ditridecylperylene-3,4,9,10-tetracarboxylic diimide (PTCDI-C13),[34,48−57] at the interface with poly-methyl metacrylate (PMMA), a polymer typically used as a dielectric layer,[6,46,58−63] in different growth and fabrication conditions, thus mimicking the configuration occurring in in-plane organic electronic devices, such as organic field-effect transistors (OFETs). Previous work indeed demonstrated that the charge transport properties and the overall performance of organic transistors depend crucially on the morphology of the active organic layer at the interface with the dielectric layer.[46] A detailed understanding with atomistic resolution of the molecular aggregation morphology at the interface with the dielectric is, therefore, required to optimize materials, architectures and processing conditions for the fabrication of efficient organic electronic devices.

We apply atomistic molecular dynamics (MD) simulations to model the structure of disordered, partially ordered, crystalline, and poly-crystalline aggregates of PTCDI-C13 at the interface with realistic models of a PMMA surface. These investigations aim at providing correlations between aggregation nanoscale morphology and local structural properties. Simulations are supported and integrated by experimental validations performed on ultra-thin films of PTCDI-C13 grown on PMMA samples, providing a unified picture of the correlation between growth conditions, post-fabrication processing, and resulting interface morphologies.

Our study underlines the role of kinetic and thermodynamic effects on the growth and interface morphology of PTCDI-C13 nanoscale aggregates at the interface with PMMA, linking our findings to the details of fabrication process. Focusing on a prototypical interface, our work highlights the potential of the computational/experimental approach proposed in the optimization growth, fabrication, and processing routes in organic electronics. The detailed understanding provided by our approach can also lead to the possibility of controlling and fine-tuning the morphology of molecular aggregates at interfaces in organic electronic devices.

## ■ METHODS

**Computational Details.** MD calculations were performed by applying a customized version of the all-atom OPLS force field,[64] taking parameters for PTCDI-C13 and PMMA from previous work.[49,65] The interaction between PTCDI-C13 and PMMA was described in terms of mixed Lennard-Jones (LJ) terms, applying standard Lorentz−Berthelot rules. Electrostatic interactions were computed by applying the particle-mesh Ewald (PME) method, using a cut-off of 10.0 Å for both Coulomb and van der Waals (LJ) interactions. The Berendsen thermostat was used for simulations in the *NVT* ensemble with a time constant of 1.0 ps. Periodic boundary conditions (PBCs) in three dimensions were used in all simulations, inserting a vacuum region of 50 Å along the $z$ direction of the box for the simulation of slabs and interfaces. The time step for all the simulations was set to 1 fs. All MD simulations were performed using the GROMACS package.[66]

The aggregation properties of the organic molecular layer are related to the morphology of the underlying polymer substrate. The definition of a realistic model of the polymer layer is, therefore, key to simulate molecular aggregation at the interface. We considered a model surface corresponding to samples obtained by spin-coating of PMMA on flat substrates, as, for example, in the fabrication of OFETs. The model of the PMMA was obtained as described in a previous work,[46] with the morphology of the exposed simulated surface comparing well with the experiment. The surface area of the PMMA model (about 10 × 10 nm) is large enough to accommodate the relaxation of large PTCDI-C13 supramolecular structures, allowing the observation of interface aggregation phenomena at the nanoscale. The thickness of the PMMA layer (about 5 nm) allows to decouple surface effects from the bulk limit. Moreover, the PMMA surface model is expected to reflect the local morphology of a PMMA sample, as shown previously.[46,67] All structures were initially relaxed to the nearest energy minimum by steepest descent optimization and subsequently equilibrated by MD.

The effect of fabrication conditions and processing on the morphology of PTCDI-C13 aggregates on a substrate was simulated by implementing MD protocols aimed at simulating growth dynamics under kinetic and thermodynamic control, respectively. Simulation of the morphology of PTCDI-C13 aggregates grown on PMMA in kinetically-controlled conditions were performed as explained in a previous work.[8] Namely, the aggregation of PTCDI-C13 molecules on PMMA in strong kinetic control was simulated by starting from the bare equilibrated PMMA substrate and adding PTCDI-C13 molecules iteratively, one by one, by applying a combination of non-equilibrium and equilibrium MD. Each PTCDI-C13 molecule is initially positioned at about 5 nm from the PMMA surface, with a random in-plane ($x$ and $y$) displacement and orientation, adding an initial velocity component of 0.5 nm ps$^{-1}$ to the $-z$ component of the velocities of all atoms. Then, a MD run is performed (100 ps), at a temperature of 300 K, allowing the PTCDI-C13 molecules to reach the PMMA surface and then relax. The procedure is repeated until reaching the target surface density. The relatively short relaxation time induces the formation of essentially amorphous aggregates.[8] In all simulations, the equilibrated final configuration exhibits a remarkably strong structural stability at 300 K in the time scale of several tens of ns. Simulations of thermodynamically stable PTCDI-C13 aggregates at the interface with PMMA were performed by equilibrating the stable configuration of PTCDI-C13 layers, as found in previous work,[48,49] in contact with the PMMA surface. Equilibrations were performed by MD at a temperature of 300 K for 50 ns. In these simulations, all equilibrated configurations were found to be structurally stable, after a relatively short (a few ns) relaxation time. Annealing of equilibrated configurations was performed by increasing the temperature of the system to 400 K, at a rate of 20 K ns$^{-1}$, equilibrating the system at 400 K for 30 ns and cooling to 300 K at a rate of 10 K ns$^{-1}$, with a final equilibration of the system at 300 K for 50 ns.

Configurations relaxed by MD were analyzed in terms of structural parameters that are relevant in the description of intermolecular and long-range aggregation of molecular materials on substrates. The overall molecular packing features were analyzed by computing the radial distribution function


https://doi.org/10.1021/acs.jpcc.3c03332
J. Phys. Chem. C 2023, 127, 18026−18035

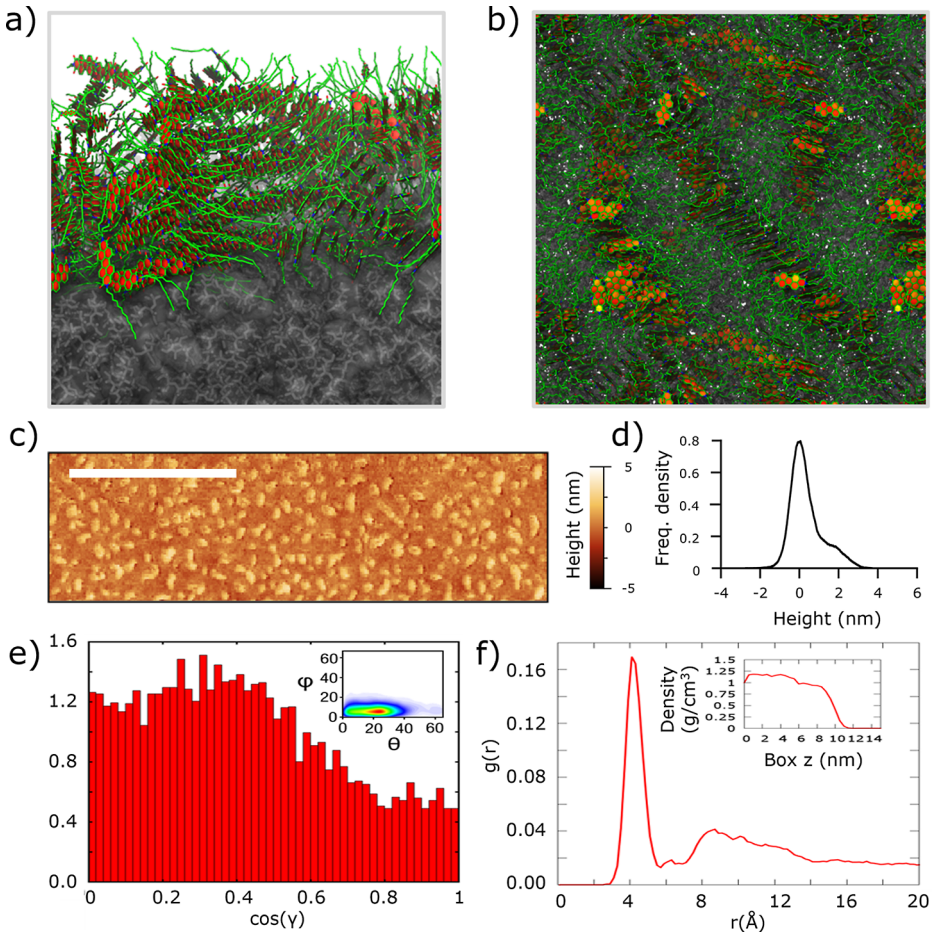


**Figure 1.** Side (a) and top (b) views of a snapshot of the MD equilibrated morphology of PTCDI-C13 (orange and green) grown on PMMA (gray) in kinetically controlled conditions. AFM topography image (c) of an as-cast sample of PTCDI-C13 grown on PMMA with a nominal coverage of 0.5 nm (scale bar: 500 nm) and height distribution across the whole sample (d). Distribution of the PTCDI-C13 tilt angles (inset: intermolecular orientation parameters) (e) and computed radial function distribution (f) for the MD equilibrated structure (inset: average density profile across the slab).

between the centers of mass of PTCDI-C13 molecules. The tilt angle $\gamma$ of PTCDI-C13 molecules was defined as the angle between the main axis of the molecule and the normal to the PMMA surface. The relative orientation between two neighboring PTCDI-C13 molecules was defined by two angular order parameters, related to the twist ($\theta$) and tilt ($\varphi$) angles between the two planes of the perylene cores, respectively. These parameters are described in detail in the Supporting Information and in previous work.[48]

**Experimental Details.** *Materials.* PTCDI-C13 was purchased by Sigma-Aldrich (CAS: 95689-92-2, MW: 755.04 mp), PMMA (AR_P 669.06) was purchased by ALLRESIST Gmbh.

*Fabrication of Organic Thin Films.* The samples were produced by sublimation on glass/ITO substrates. The glass/ITO substrates underwent to multistep washing process in ultrasonic bath with acetone and isopropanol alcohol, each step lasting 15 min at room temperature. The PMMA layer (450 nm) was deposited on top of the glass/ITO substrate by spin coating and then annealed at 353 K. The PTCDI-C13 layer was sublimated in vacuum on the glass/ITO/PMMA stack at a growth rate of 0.6 nm/min. The thickness of PTCDI-C13 layers vary from 0.5 to 2 nm and it is measured by a quartz microbalance. All samples were annealed on a hotplate at 328 K for 40 min following the deposition of PTCDI-C13.

*AFM Imaging.* AFM micrographs were acquired under nitrogen with SNL-A probes (Bruker, USA) having a nominal tip radius of 2−12 nm and a nominal elastic constant of ∼0.35 N $m^{-1}$ on a Multimode8 microscope (Bruker, USA) equipped with a Nanoscope V controller and a type J piezoelectric scanner, operated in PeakForce mode at an applied force of ≤250 pN and a lateral velocity ≤ 1 $\mu$m $s^{-1}$. Background subtraction and image analysis were performed with Gwyddion 2.61.[68] AFM analyses were performed before and after the annealing process.

## RESULTS AND DISCUSSION

The properties of PTCDI-C13 aggregates at the interface with PMMA were simulated by different protocols, as described in the Methods section, addressing the relationship between growth conditions, processing, and resulting morphology. In kinetically controlled growth conditions, PTCDI-C13 aggregates formed at the interface with planar or quasi-planar substrates typically exhibit a mostly amorphous morphology.[69] The simulation conditions applied reflect the growth of PTCDI-C13 on substrates at high growth rates and at room temperature. In Figure 1, a snapshot of the equilibrated configuration obtained from simulations of the growth of PTCDI-C13 on PMMA in kinetically controlled conditions, up to a coverage of 3.0 mol $nm^2$, is shown.

The overall simulated aggregation structure (see Figure 1a,b) evidences a largely amorphous morphology of PTCDI-C13 at the interface with PMMA, with local molecular packing in different directions, in agreement with previous work.[69] AFM


https://doi.org/10.1021/acs.jpcc.3c03332
J. Phys. Chem. C 2023, 127, 18026−18035

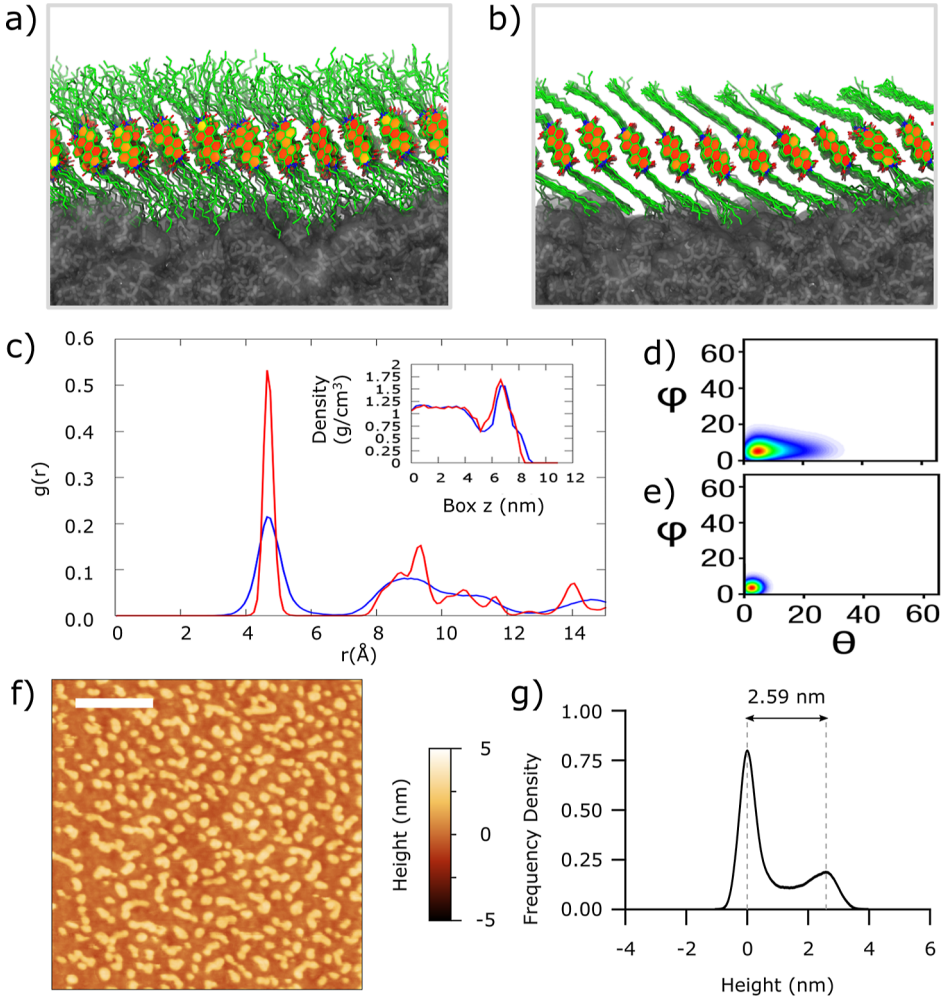


**Figure 2.** Snapshot of the MD morphology of a PTCDI-C13 layer in the CF configuration (orange and green) equilibrated on PMMA (gray) relaxed at 300 K (a) and after annealing at 400 K (b). Computed radial function distribution (c) for the MD equilibrated structures (blue: unannealed configuration; red: annealed configuration; inset: average density profile across the slab). Intermolecular orientation parameters for the unannealed (d) and annealed (e) configuration. AFM topography image (f) of a fully relaxed sample of PTCDI-C13 grown on PMMA with a nominal coverage of 0.5 nm (scalebar: 500 nm) and height distribution across the whole sample (g).

topography (see Figure 1c,d) of an as-cast (unrelaxed) layer of PTCDI-C13 with nominal height of 0.5 nm grown on PMMA shows a distribution of heights (about 1.8 nm) that is lower than that expected for a complete monolayer. The measured averaged height profile shows a broad distribution, pointing to a largely unstructured aggregation. In agreement with simulations, this distribution indicates a likely loose packing, with most of the molecules arranged differently from the expected crystalline stand-up phase.

Increasing the nominal coverage of PTCDI-C13 on PMMA to 1 nm, in the same growth conditions, leads to only slightly more structured aggregation (see Figure S1 in the Supporting Information). The morphology of the PTCDI-C13 layer does not provide evidence of formation of long-range ordered structures with a particular alignment with respect to the PMMA surface, as, for example, in islands and terraces. However, a deeper analysis of the simulated interface morphology suggests the occurrence of local structuration of PTCDI-C13 aggregates. Despite a scattered range of molecular orientations with respect to the underlying surface (see Figure 1e), the analysis of the intermolecular orientation in nearest-neighbor dimers (see Figure 1e, inset) shows a strong tendency to local aggregation of PTCDI-C13 molecules in a staggered (ST) configuration, which is a metastable phase for bulk and 2D structures.[48] The pair correlation function between the molecular centers of mass (see Figure 1f) and the density profile of PTCDI-C13 molecules at the interface (see Figure 1f, inset) shows a tight molecular packing, peaked at a distance (about 4 Å) that is compatible with close intermolecular $\pi-\pi$ stacking. Moreover, simulations indicate the occurrence of long-range alignment of molecules along the axis perpendicular to the molecular $\pi$-system, at different orientations with respect to the substrate. In kinetically controlled conditions, therefore, the growth dynamics leads to preferential growth of PTCDI-C13 aggregates in the direction perpendicular to the most stable surface ([001]) of the bulk crystal, that is, perpendicular to the $\pi$-stacking plane, without a particular alignment of aggregates with respect to the underlying PMMA surface. This driving force leads, at larger coverages, to the formation of three-dimensional needle-like aggregates of PTCDI-C13, which are often observed in experiments.[69,70]

In thermodynamically controlled conditions, the formation of more ordered aggregates of standing-up molecules of PTCDI-C13 at the interfaces is expected. The thermodynamically most


https://doi.org/10.1021/acs.jpcc.3c03332
J. Phys. Chem. C 2023, 127, 18026−18035

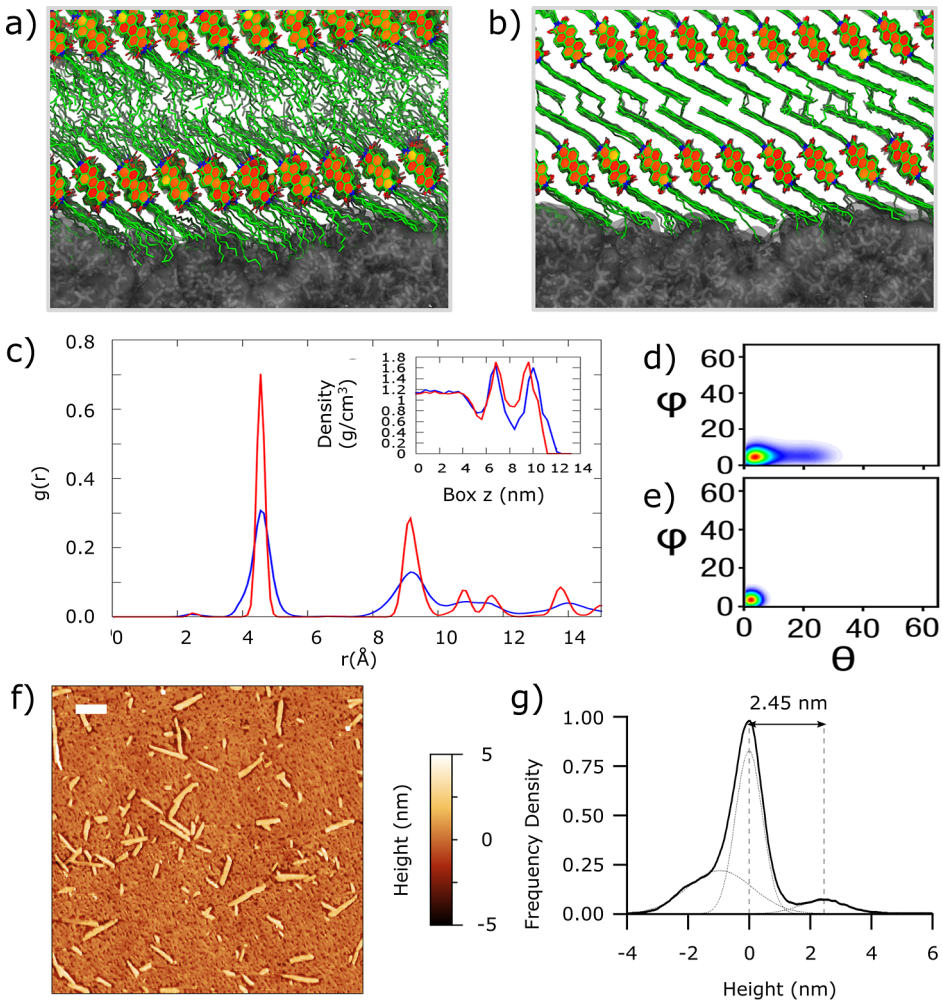


**Figure 3.** Snapshot of the MD simulated morphology of a PTCDI-C13 bilayer in the CF configuration (orange and green) equilibrated on PMMA (gray) relaxed at 300 K (a) and after annealing at 400 K (b). Computed radial function distribution (c) for the MD equilibrated structures (blue: unannealed configuration; red: annealed configuration; inset: average density profile across the slab). Intermolecular orientation parameters for the unannealed (d) and annealed (e) configuration. AFM topography image (f) of an annealed sample of PTCDI-C13 grown on PMMA with a nominal coverage of 2.0 nm (scalebar: 500 nm) and height distribution across the whole sample (g).

stable phase of a PTCDI-C13 monolayer, in both free-standing and supported conditions, is a co-facial (CF) phase, as previously demonstrated by calculations and experiments.[48,50,71,72] The relaxed simulated structure of a PTCDI-C13 monolayer in the CF phase equilibrated by MD on the PMMA surface is shown in Figure 2a. Simulations indicate a remarkable long-range crystal ordering and tight packing (see Figure 2c,d) of PTCDI-C13 molecules at the interface, despite the roughness of the underlying PMMA surface. The computed rms roughness of the exposed surface lowers from 0.50 nm for the bare PMMA[46] surface to 0.20 nm for the surface of the PTCDI-C13 monolayer on PMMA. As shown by the MD snapshot of Figure 2a, the long-range structural ordering of PTCDI-C13 molecules in the CF monolayer phase on PMMA is assisted by the flexibility of the side alkyl chains, which adapt to the surface, while keeping intact strong $\pi$-stacking intermolecular interactions, confirming the observations of previous work.[49] Remarkably, MD also evidences the effect of thermal treatments on the PTCDI-C13 monolayer on PMMA in improving long-range ordering. Namely, by performing annealing simulations of the PTCDI-C13 layer at a target temperature of 400 K (see Computational Details), a long-range alignment of the PTCDI-C13 alkyl chains is observed (see Figure 2b), which is also reflected in improved short-range packing (see Figure 2c,e).

Experiments were performed on the relaxation of PTCDI-C13 on PMMA at a nominal coverage of 0.5 nm. After an initial thermal equilibration at room temperature for 24 h, we observed that consecutive applications of the AFM tip on the sample led to increasingly ordered packing (see Figure S2 in the Supporting Information). These intermediate aggregation morphologies are structurally stable upon thermal annealing at 328 K for 40 min (see Figures S3 and S4 in the Supporting Information). Therefore, the combined effect of thermal and tip-induced relaxation is able to drive aggregation toward ordered morphologies.

The height of the PTCDI-C13 islands on PMMA, measured after a 24 h relaxation at room temperature and four successive passes of the AFM tip (2.59 nm, see Figure 2f,g), is in excellent agreement with the height of PTCDI-C13 layers obtained by simulations (2.56 nm). These findings also align with previous research.[69]

The application of thermal processes to the samples of PTCDI-C13 on PMMA in the sub-monolayer regime can


https://doi.org/10.1021/acs.jpcc.3c03332
J. Phys. Chem. C 2023, 127, 18026−18035

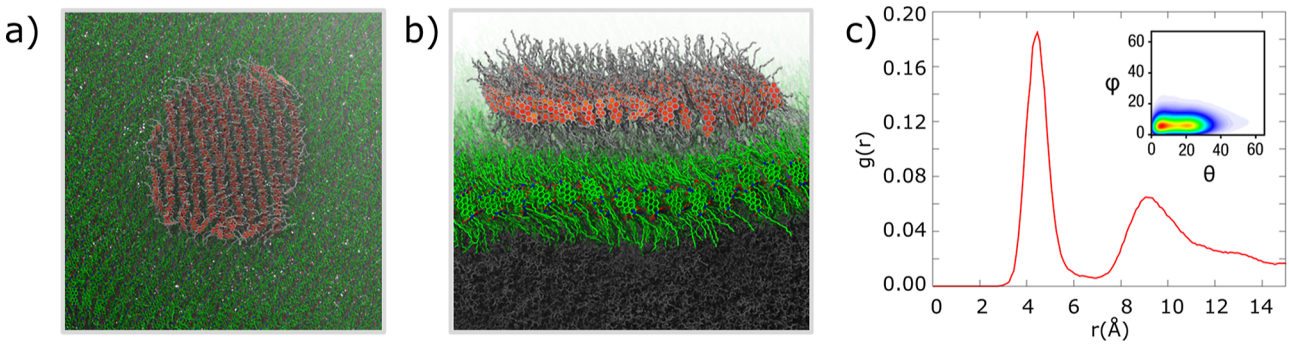


**Figure 4.** Snapshot of the MD simulated morphology of an island of PTCDI-C13 (orange and gray) equilibrated on a PTCDI-C13 monolayer (green) supported on PMMA (gray) [top (a) and side (b) views]. (c) Computed radial function distribution for the PTCDI-C13 molecules of the island (inset: intermolecular orientation parameters).

indeed affect the dynamics of structural reorganizations at the interface including modifications of the polymer surface induced by heating. Although the case is different from that of complete layers, as in devices, the occurrence of different morphologies underscores the role of processing (as evidenced by the effect of thermal annealing compared to the tip-induced aggregation discussed above) in determining the morphology of PTCDI-C13 aggregates on substrates. Post-growth processing of PTCDI-C13 thin-films on PMMA and thermal treatments can, therefore, affect significantly the interface morphology and related properties, improving both intermolecular local packing and long-range aggregation. In particular, annealing of PTCDI-C13 aggregates on PMMA can be expected to improve significantly the charge transport properties of the organic layer.

A similar effect is observed for bilayers of PTCDI-C13, in the CF configuration, relaxed on PMMA (see Figure 3a) in conditions that can be expected for thermodynamically controlled growth. In bilayers, post-growth simulated thermal annealing improves both intermolecular and inter-layer packing (see Figure 3b−d), driven by the relaxation of side alkyl chains. The distribution of heights for samples grown with a nominal coverage of 2 nm measured experimentally (see Figure 3f,g) supports the picture provided by computational models. The unrelaxed samples correspond to an almost complete layer of PTCDI-C13 in the CF phase (85 ± 6% coverage) and an overlayer of small regions corresponding to a second monolayer.

Interestingly, the experimentally measured overall surface coverage, at the nominal coverage of 2 nm, is only 1.4 times larger than the value observed at 1 nm (61 ± 1% coverage), computed from the same growth rate. Nominal coverages are indeed computed from deposition times by assuming constant growth rates for all samples. This assumption does not take into account the affinity between the grown species (PTCDI-C13) and the nature of the surface, thus introducing a strong bias in the relationship between nominal and real coverages. As we observe a much smaller coverage than expected we can assume that, in these growth conditions, PTCDI-C13 molecules exhibit a larger affinity toward PMMA with respect to PTCDI-C13 layers.

A comparable effect of thermal annealing in improving the packing of PTCDI-C13 bilayers is also observed in the simulation of other metastable phases, such as interdigitated structures (see Figure S5 in the Supporting Information).

In ordinary growth conditions, organic molecular aggregates of PTCDI-C13 usually exhibit a polycrystalline structure, related to the occurrence of concurrent nucleation events. At low coverages, individual molecules first aggregate to form islands, according to a crystalline structural motif. By increasing coverage, islands get into contact with each other, leading eventually to a polycrystalline complete monolayer. One of the crucial aspects of molecular interface engineering concerns, therefore, the relationship between the structure of crystalline phases and the local morphology of islands and polycrystalline aggregates. To investigate the structural properties of islands of PTCDI-C13, MD simulations were performed on model systems constituted by nanoscale molecular aggregates at the interface with PMMA. Free-standing islands of PTCDI-C13 in the CF phase, with a diameter of about 5 nm, are stable at room temperature in vacuum, as shown in previous work.[48] By thermal equilibration, the free-standing PTCDI-C13 islands assume generally a rounded shape and retain the crystal packing of the stable CF phase. However, simulations show that PTCDI-C13 islands with a similar size (about 5 nm diameter) relaxed on PMMA are unstable under MD at room temperature, and tend to collapse onto the underlying surface. In this case, the size of the molecular cluster is, therefore, too small to compensate for the molecule−surface interaction with intermolecular packing forces, as a consequence of the small ratio between the number of close-packed (bulk-like) molecules and molecules at the edge. The affinity of PTCDI-C13 molecules toward PMMA can be related to the aliphatic interactions between the molecular components and the exposed polymer units. These interactions can also account for the mechanical energy needed to achieve full relaxation of PTCDI-C13 aggregates in the thermodynamically most stable phase, as observed above. In contrast, small PTCDI-C13 islands on top of a complete monolayer of PTCDI-C13 molecules supported on PMMA exhibit remarkable stability in the time scale of MD simulations (see Figure 4).

Upon equilibration, PTCDI-C13 islands at the interface with PTCDI-C13 monolayers take initially a rounded shape, irrespective of the initial symmetry of the molecular cluster, in agreement with the experiment.[70] The height of the equilibrated island (2.56 nm) is also in excellent agreement with the terrace height observed in experiments. Structural parameters indicate that, despite the overall apparent shape, the close packing of the CF phase is essentially maintained in PTCDI-C13 islands at interfaces, which are, therefore, constituted by monocrystalline aggregates, with a slightly lower density with respect to that of a complete monolayer. In our simulations, we found different likely orientations of equilibrated PTCDI-C13 islands over the organic monolayer, as a result of the weak forces between the alkyl chains of the two layers. However, the epitaxial (aligned) arrangement of the PTCDI-C13 island with respect to the


https://doi.org/10.1021/acs.jpcc.3c03332
J. Phys. Chem. C 2023, 127, 18026−18035

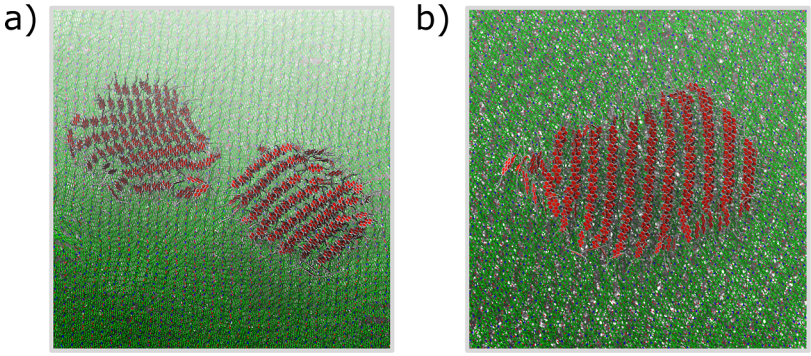


**Figure 5.** Snapshot of the MD simulated morphology of two islands of PTCDI-C13 (orange and gray) equilibrated on a PTCDI-C13 monolayer (green) supported on PMMA after 10 (a) and 50 ns (b) of simulation.

underlying CF layer, similar to the bilayer structure of Figure 2, is expected to be energetically favored.

The growth of a complete monolayer of PTCDI-C13 molecules from islands is expected to lead to the formation of polycrystalline aggregates. However, collective diffusion of PTCDI-C13 molecules on surfaces can lead to aggregation by coalescence. The coalescence of neighboring PTCDI-C13 islands can be related to surface diffusion and, as such, is triggered by kinetic energy. To simulate the dynamics of PTCDI-C13 islands at interfaces, we equilibrated two aggregates of PTCDI-C13 molecules in the CF phase, with a diameter of about 5 nm, at a distance of about 5 nm from each other, and randomly oriented with respect to the underlying PTCDI-C13 monolayer, supported on PMMA. After about 10 ns of equilibration at room temperature, both clusters acquire the rounded shape observed previously and get closer to each other, as a consequence of thermal molecular diffusion on the surface (see Figure 5a).

Upon further equilibration, the two islands get in contact, forming a grain boundary (see the Movie S1 in the Supporting Information). However, in the time scale of about 10 ns, complete coalescence of the two islands into each other is observed (see Figure 5b), with formation of an ordered aggregate in the CF phase. The possible occurrence of coalescence phenomena upon thermal annealing is also signaled experimentally by the change in the mean area of islands measured by AFM, which increases from 2600 to 22,000 $nm^2$ in PTCDI-C13 samples on PMMA with nominal coverage of 2 nm (see Figures 3f and S6 in the Supporting Information). Remarkably, molecules in the coalesced and relaxed nanostructure are epitaxially aligned with respect to the underlying layer of PTCDI-C13 molecules (see Figure 5b). The propensity of PTCDI-C13 overlayers to aggregate along the $\pi-\pi$ stacking direction compares well with the elongated shape of PTCDI-C13 nanostructures on monolayers observed experimentally (see Figure 3). The packing of the PTCDI-C13 island formed by coalescence strongly exhibits the CF aggregation, with a few ST aggregates at the edges of the island, as can also be observed from the orientational parameters (see Figure S7 in the Supporting Information). Coalescence processes may, therefore, lead to a significant structural smoothing between neighboring islands of PTCDI-C13 on surfaces and are expected to improve in-plane charge mobility and to reduce greatly the occurrence of trap states related to defects and grain boundaries.

## CONCLUSIONS

In this work, we investigated the morphology of PTCDI-C13 layers on PMMA through joint computational and experimental investigations. Our study highlights the role of fabrication and post-processing conditions in the definition of aggregation and packing at the molecular level, which impacts the overall properties of PTCDI-C13 thin films. Stable and ordered PTCDI-C13 aggregates at the interface with PMMA typically exhibit a face-to-face configuration, with upstanding individual molecules. Both simulations and experiments suggest a significant improvement of long-range packing order of PTCDI-C13 aggregates at the interface upon thermal annealing. Accordingly, thermal processes enhance a layer-by-layer growth in the initial stages of the deposition of PTCDI-C13 films on PMMA. The significant packing order is also evidenced by the strong correlation between nominal and effective coverage, with uniform distribution of layer heights that corresponds to the height of ordered aggregates of PTCDI-C13 molecules in the co-facial standing-up phase. Moreover, thermal annealing can also improve in-plane ordering, assisting the coalescence of PTCDI-C13 islands toward the formation of larger aggregates with extended crystalline order. Although the effect of annealing and thermal processes in thicker films and full-scale devices may be linked to several other factors, this work emphasizes fundamental aspects in the correlation between processing and morphology at the interface between PTCDI-C13 and PMMA.

## ASSOCIATED CONTENT

### Supporting Information

The Supporting Information is available free of charge at https://pubs.acs.org/doi/10.1021/acs.jpcc.3c03332.

Simulation and AFM data of PTCDI-C13 aggregates on PMMA not included in the text (PDF)

A movie of the dynamics of the coalescence between two supported islands of PTCDI-C13 (MP4)

## AUTHOR INFORMATION

### Corresponding Author

**Francesco Mercuri** − *Istituto per lo Studio dei Materiali Nanostrutturati (ISMN), Consiglio Nazionale delle Ricerche (CNR), 40129 Bologna, Italy;* orcid.org/0000-0002-3369-4438; Phone: +39 (0)51 6398518; Email: francesco.mercuri@cnr.it; Fax: +39 (0)51 6398540



https://doi.org/10.1021/acs.jpcc.3c03332
J. Phys. Chem. C 2023, 127, 18026−18035

## Authors

**Andrea Lorenzoni** − *Istituto per lo Studio dei Materiali Nanostrutturati (ISMN), Consiglio Nazionale delle Ricerche (CNR), 40129 Bologna, Italy*

**Federico Prescimone** − *Istituto per lo Studio dei Materiali Nanostrutturati (ISMN), Consiglio Nazionale delle Ricerche (CNR), 40129 Bologna, Italy*

**Marco Brucale** − *Istituto per lo Studio dei Materiali Nanostrutturati (ISMN), Consiglio Nazionale delle Ricerche (CNR), 40129 Bologna, Italy;* orcid.org/0000-0001-7244-4389

**Stefano Toffanin** − *Istituto per lo Studio dei Materiali Nanostrutturati (ISMN), Consiglio Nazionale delle Ricerche (CNR), 40129 Bologna, Italy;* orcid.org/0000-0003-4099-8664

Complete contact information is available at: https://pubs.acs.org/10.1021/acs.jpcc.3c03332


## Notes

The authors declare no competing financial interest.

## ■ ACKNOWLEDGMENTS

The authors thank Federico Bona (CNR-ISMN) for technical support. The authors also acknowledge the CINECA supercomputing center (Bologna, Italy).

## ■ REFERENCES


(1) Fahlman, M.; Fabiano, S.; Gueskine, V.; Simon, D.; Berggren, M.; Crispin, X. Interfaces in organic electronics. *Nat. Rev. Mater.* **2019**, *4*, 627−650.

(2) Koch, N. Organic electronic devices and their functional interfaces. *ChemPhysChem* **2007**, *8*, 1438−1455.

(3) Ma, H.; Yip, H. L.; Huang, F.; Jen, A. K. Interface engineering for organic electronics. *Adv. Funct. Mater.* **2010**, *20*, 1371−1388.

(4) Li, P.; Lu, Z.-H. Interface Engineering in Organic Electronics: Energy-Level Alignment and Charge Transport. *Small Sci.* **2021**, *1*, 2000015.

(5) Liao, C.; Zhang, M.; Yao, M. Y.; Hua, T.; Li, L.; Yan, F. Flexible Organic Electronics in Biology: Materials and Devices. *Adv. Mater.* **2015**, *27*, 7493−7527.

(6) Natali, M.; Prosa, M.; Longo, A.; Brucale, M.; Mercuri, F.; Buonomo, M.; Lago, N.; Benvenuti, E.; Prescimone, F.; Bettini, C.; et al. On the Nature of Charge-Injecting Contacts in Organic Field-Effect Transistors. *ACS Appl. Mater. Interfaces* **2020**, *12*, 30616−30626.

(7) Friederich, P.; Fediai, A.; Kaiser, S.; Konrad, M.; Jung, N.; Wenzel, W. Toward Design of Novel Materials for Organic Electronics. *Adv. Mater.* **2019**, *31*, 1808256.

(8) Lorenzoni, A.; Muccini, M.; Mercuri, F. A Computational Predictive Approach for Controlling the Morphology of Functional Molecular Aggregates on Substrates. *Adv. Theory Simul.* **2019**, *2*, 1900156.

(9) Lorenzoni, A.; Mosca Conte, A.; Pecchia, A.; Mercuri, F. Nanoscale morphology and electronic coupling at the interface between indium tin oxide and organic molecular materials. *Nanoscale* **2018**, *10*, 9376−9385.

(10) Han, G.; Yi, Y.; Shuai, Z. From Molecular Packing Structures to Electronic Processes: Theoretical Simulations for Organic Solar Cells. *Adv. Energy Mater.* **2018**, *8*, 1702743.

(11) Li, Q.; Li, Z. Molecular Packing: Another Key Point for the Performance of Organic and Polymeric Optoelectronic Materials. *Acc. Chem. Res.* **2020**, *53*, 962−973.

(12) Luo, Z.; Ma, R.; Xiao, Y.; Liu, T.; Sun, H.; Su, M.; Guo, Q.; Li, G.; Gao, W.; Chen, Y.; et al. Conformation-Tuning Effect of Asymmetric Small Molecule Acceptors on Molecular Packing, Interaction, and Photovoltaic Performance. *Small* **2020**, *16*, 2001942.

(13) Prosa, M.; Moschetto, S.; Benvenuti, E.; Zambianchi, M.; Muccini, M.; Melucci, M.; Toffanin, S. 2,3-Thienoimide-ended oligothiophenes as ambipolar semiconductors for multifunctional single-layer light-emitting transistors. *J. Mater. Chem. C* **2020**, *8*, 15048.

(14) Diao, Y.; Lenn, K. M.; Lee, W. Y.; Blood-Forsythe, M. A.; Xu, J.; Mao, Y.; Kim, Y.; Reinspach, J. A.; Park, S.; Aspuru-Guzik, A.; et al. Understanding polymorphism in organic semiconductor thin films through nanoconfinement. *J. Am. Chem. Soc.* **2014**, *136*, 17046−17057.

(15) Riera-Galindo, S.; Tamayo, A. A.; Mas-Torrent, M. Role of Polymorphism and Thin-Film Morphology in Organic Semiconductors Processed by Solution Shearing. *ACS Omega* **2018**, *3*, 2329−2339.

(16) Brown, R. D.; Corcelli, S. A.; Kandel, S. A. Structural Polymorphism as the Result of Kinetically Controlled Self-Assembly. *Acc. Chem. Res.* **2018**, *51*, 465−474.

(17) Chung, H.; Diao, Y. Polymorphism as an emerging design strategy for high performance organic electronics. *J. Mater. Chem. C* **2016**, *4*, 3915−3933.

(18) Jones, A. O.; Chattopadhyay, B.; Geerts, Y. H.; Resel, R. Substrate-induced and thin-film phases: Polymorphism of organic materials on surfaces. *Adv. Funct. Mater.* **2016**, *26*, 2233−2255.

(19) Casalini, S.; Bortolotti, C. A.; Leonardi, F.; Biscarini, F. Self-assembled monolayers in organic electronics. *Chem. Soc. Rev.* **2017**, *46*, 40−71.

(20) Melucci, M.; Durso, M.; Bettini, C.; Gazzano, M.; Maini, L.; Toffanin, S.; Cavallini, S.; Cavallini, M.; Gentili, D.; Biondo, V.; et al. Structure-property relationships in multifunctional thieno(bis)imide-based semiconductors with different sized and shaped N-alkyl ends. *J. Mater. Chem. C* **2014**, *2*, 3448−3456.

(21) Someya, T.; Bao, Z.; Malliaras, G. G. The rise of plastic bioelectronics. *Nature* **2016**, *540*, 379−385.

(22) Weitz, R. T.; Amsharov, K.; Zschieschang, U.; Villas, E. B.; Goswami, D. K.; Burghard, M.; Dosch, H.; Jansen, M.; Kern, K.; Klauk, H. Organic n-Channel Transistors Based on Core-Cyanated Perylene Carboxylic Diimide Derivatives. *J. Am. Chem. Soc.* **2008**, *130*, 4637−4645.

(23) Zhang, X.; Barrena, E.; Goswami, D.; De Oteyza, D. G.; Weis, C.; Dosch, H. Evidence for a Layer-Dependent Ehrlich-Schwöbel Barrier in Organic Thin Film Growth. *Phys. Rev. Lett.* **2009**, *103*, 136101.

(24) Di, C.-A.; Liu, Y.; Yu, G.; Zhu, D. Interface Engineering: An Effective Approach toward High-Performance Organic Field-Effect Transistors. *Acc. Chem. Res.* **2009**, *42*, 1573−1583.

(25) Perez-Rodríguez, A.; Temiño, I.; Ocal, C.; Mas-Torrent, M.; Barrena, E. Decoding the Vertical Phase Separation and Its Impact on C8-BTBT/PS Transistor Properties. *ACS Appl. Mater. Interfaces* **2018**, *10*, 7296−7303.

(26) Witte, G.; Wöll, C. Growth of aromatic molecules on solid substrates for applications in organic electronics. *J. Mater. Res.* **2004**, *19*, 1889−1916.

(27) Viani, L.; Risko, C.; Toney, M. F.; Breiby, D. W.; Brédas, J.-L. Substrate-Induced Variations of Molecular Packing, Dynamics, and Intermolecular Electronic Couplings in Pentacene Monolayers on the Amorphous Silica Dielectric. *ACS Nano* **2014**, *8*, 690−700.

(28) Li, L.; Hu, W.; Fuchs, H.; Chi, L. Controlling molecular packing for charge transport in organic thin films. *Adv. Energy Mater.* **2011**, *1*, 188−193.

(29) Shtein, M.; Mapel, J.; Benziger, J. B.; Forrest, S. R. Effects of film morphology and gate dielectric surface preparation on the electrical characteristics of organic-vapor-phase-deposited pentacene thin-film transistors. *Appl. Phys. Lett.* **2002**, *81*, 268−270.

(30) Han, G.; Shen, X.; Yi, Y. Deposition Growth and Morphologies of C60 on DTDCTB Surfaces: An Atomistic Insight into the Integrated Impact of Surface Stability, Landscape, and Molecular Orientation. *Adv. Mater. Interfaces* **2015**, *2*, 1500329.

(31) Perez-Rodriguez, A.; Barrena, E.; Fernández, A.; Gnecco, E.; Ocal, C. A molecular-scale portrait of domain imaging in organic surfaces. *Nanoscale* **2017**, *9*, 5589−5596.

(32) Kumar, P.; Shivananda, K. N.; Zajaczkowski, W.; Pisula, W.; Eichen, Y.; Tessler, N. The relation between molecular packing or

morphology and chemical structure or processing conditions: The effect on electronic properties. *Adv. Funct. Mater.* **2014**, *24*, 2530−2536.
(33) Fitzner, R.; Mena-Osteritz, E.; Mishra, A.; Schulz, G.; Reinold, E.; Weil, M.; Körner, C.; Ziehlke, H.; Elschner, C.; Leo, K.; et al. Correlation of π-Conjugated Oligomer Structure with Film Morphology and Organic Solar Cell Performance. *J. Am. Chem. Soc.* **2012**, *134*, 11064−11067.
(34) Jang, M.; Baek, K. Y.; Yang, H. Optimization of Temperature-Mediated Organic Semiconducting Crystals on Soft Polymer-Treated Gate Dielectrics. *J. Phys. Chem. C* **2013**, *117*, 25290−25297.
(35) Benvenuti, E.; Gentili, D.; Chiarella, F.; Portone, A.; Barra, M.; Cecchini, M.; Cappuccino, C.; Zambianchi, M.; Lopez, S. G.; Salzillo, T.; et al. Tuning polymorphism in 2,3-thienoimide capped oligothiophene based field-effect transistors by implementing vacuum and solution deposition methods. *J. Mater. Chem. C* **2018**, *6*, 5601−5608.
(36) Baldoni, M.; Lorenzoni, A.; Pecchia, A.; Mercuri, F. Spatial and orientational dependence of electron transfer parameters in aggregates of iridium-containing host materials for OLEDs: Coupling constrained density functional theory with molecular dynamics. *Phys. Chem. Chem. Phys.* **2018**, *20*, 28393−28399.
(37) Prescimone, F.; Benvenuti, E.; Natali, M.; Lorenzoni, A.; Dinelli, F.; Liscio, F.; Milita, S.; Chen, Z.; Mercuri, F.; Muccini, M.; et al. 3D versus 2D Electrolyte−Semiconductor Interfaces in Rylenediimide-Based Electron-Transporting Water-Gated Organic Field-Effect Transistors. *Adv. Electron. Mater.* **2020**, *6*, 2000638.
(38) Wang, S.; Fabiano, S.; Himmelberger, S.; Puzinas, S.; Crispin, X.; Salleo, A.; Berggren, M. Experimental evidence that short-range intermolecular aggregation is sufficient for efficient charge transport in conjugated polymers. *Proc. Natl. Acad. Sci. U.S.A.* **2015**, *112*, 10599−10604.
(39) Kim, K.-H.; Yu, H.; Kang, H.; Kang, D. J.; Cho, C. H.; Cho, H.-H.; Oh, J. H.; Kim, B. J. Influence of intermolecular interactions of electron donating small molecules on their molecular packing and performance in organic electronic devices. *J. Mater. Chem. A* **2013**, *1*, 14538−14547.
(40) Ye, L.; Weng, K.; Xu, J.; Du, X.; Chandrabose, S.; Chen, K.; Zhou, J.; Han, G.; Tan, S.; Xie, Z.; et al. Unraveling the influence of non-fullerene acceptor molecular packing on photovoltaic performance of organic solar cells. *Nat. Commun.* **2020**, *11*, 6005.
(41) Jeong, E.; Ito, T.; Takahashi, K.; Koganezawa, T.; Hayashi, H.; Aratani, N.; Suzuki, M.; Yamada, H. Exploration of Alkyl Group Effects on the Molecular Packing of 5,15-Disubstituted Tetrabenzoporphyrins toward Efficient Charge-Carrier Transport. *ACS Appl. Mater. Interfaces* **2022**, *14*, 32319−32329.
(42) Song, C. E.; Kim, Y. J.; Suranagi, S. R.; Kini, G. P.; Park, S.; Lee, S. K.; Shin, W. S.; Moon, S. J.; Kang, I. N.; Park, C. E.; et al. Impact of the Crystalline Packing Structures on Charge Transport and Recombination via Alkyl Chain Tunability of DPP-Based Small Molecules in Bulk Heterojunction Solar Cells. *ACS Appl. Mater. Interfaces* **2016**, *8*, 12940−12950.
(43) Kupgan, G.; Chen, X.-K.; Brédas, J.-L. Molecular Packing in the Active Layers of Organic Solar Cells Based on Non-Fullerene Acceptors: Impact of Isomerization on Charge Transport, Exciton Dissociation, and Nonradiative Recombination. *ACS Appl. Energy Mater.* **2021**, *4*, 4002−4011.
(44) Benvenuti, E.; Portale, G.; Brucale, M.; Quiroga, S. D.; Baldoni, M.; MacKenzie, R. C.; Mercuri, F.; Canola, S.; Negri, F.; Lago, N.; et al. Beyond the 2D Field-Effect Charge Transport Paradigm in Molecular Thin-Film Transistors. *Adv. Electron. Mater.* **2023**, *9*, 2200547.
(45) Bansal, A. K.; Sajjad, M. T.; Antolini, F.; Stroea, L.; Gečys, P.; Raciukaitis, G.; André, P.; Hirzer, A.; Schmidt, V.; Ortolani, L.; et al. In situ formation and photo patterning of emissive quantum dots in small organic molecules. *Nanoscale* **2015**, *7*, 11163−11172.
(46) Lorenzoni, A.; Muccini, M.; Mercuri, F. Correlation between gate-dielectric morphology at the nanoscale and charge transport properties in organic field-effect transistors. *RSC Adv.* **2015**, *5*, 11797−11805.
(47) Selli, D.; Baldoni, M.; Sgamellotti, A.; Mercuri, F. Redox-switchable devices based on functionalized graphene nanoribbons. *Nanoscale* **2012**, *4*, 1350−1354.
(48) Lorenzoni, A.; Gallino, F.; Muccini, M.; Mercuri, F. Theoretical insights on morphology and charge transport properties of two-dimensional: N, N'-ditridecylperylene-3,4,9,10-tetra carboxylic diimide aggregates. *RSC Adv.* **2016**, *6*, 40724−40730.
(49) Lorenzoni, A.; Muccini, M.; Mercuri, F. Morphology and Electronic Properties of N,N'-Ditridecylperylene-3,4,9,10-tetracarboxylic Diimide Layered Aggregates: From Structural Predictions to Charge Transport. *J. Phys. Chem. C* **2017**, *121*, 21857−21864.
(50) Tatemichi, S.; Ichikawa, M.; Koyama, T.; Taniguchi, Y. High mobility n-type thin-film transistorsbased on N,N'-ditridecyl perylene diimidewith thermal treatments. *Appl. Phys. Lett.* **2006**, *89*, 112108.
(51) Roh, J.; Lee, J.; Kang, C.-M.; Lee, C.; Jung, B. J. Air stability of PTCDI-C13-based n-OFETs on polymer interfacial layers. *Phys. Status Solidi RRL* **2013**, *7*, 469−472.
(52) Wang, Y.; Lu, C.; Kang, L.; Shang, S.; Yin, J.; Gao, X.; Yuan, G.; Xia, Y.; Liu, Z. Enhanced Performance of Organic Field-Effect Transistor Memory by Hole-Barrier Modulation with an N-Type Organic Buffer Layer between Pentacene and Polymer Electret. *Adv. Electron. Mater.* **2020**, *6*, 1901184.
(53) Wu, L.; Yu, T.; Liu, Z.; Wang, Y.; Wan, Z. T.; Yin, J.; Xia, Y.; Liu, Z. High-performance flexible pentacene transistor memory with PTCDI-C13 as N-type buffer layer. *Semicond. Sci. Technol.* **2023**, *38*, 025010.
(54) Muccini, M. A bright future for organic fi eld-effect transistors. *Nat. Mater.* **2006**, *5*, 605−613.
(55) Capelli, R.; Amsden, J. J.; Generali, G.; Toffanin, S.; Benfenati, V.; Muccini, M.; Kaplan, D. L.; Omenetto, F. G.; Zamboni, R. Integration of silk protein in organic and light-emitting transistors. *Org. Electron.* **2011**, *12*, 1146−1151.
(56) Toffanin, S.; Benfenati, V.; Pistone, A.; Bonetti, S.; Koopman, W.; Posati, T.; Sagnella, A.; Natali, M.; Zamboni, R.; Ruani, G.; et al. N-type perylene-based organic semiconductors for functional neural interfacing. *J. Mater. Chem. B* **2013**, *1*, 3850−3859.
(57) Koopman, W. A.; Natali, M.; Donati, G. P.; Muccini, M.; Toffanin, S. ChargeExciton Interaction Rate in Organic Field-Effect Transistors by Means of Transient Photoluminescence Electro-modulated Spectroscopy. *ACS Photonics* **2017**, *4*, 282−291.
(58) Wang, S.; Wang, Z.; Li, J.; Li, L.; Hu, W. Surface-grafting polymers: From chemistry to organic electronics. *Mater. Chem. Front.* **2020**, *4*, 692−714.
(59) Dao, T. T.; Sakai, H.; Ohkubo, K.; Fukuzumi, S.; Murata, H. Low switching voltage, high-stability organic phototransistor memory based on a photoactive dielectric and an electron trapping layer. *Org. Electron.* **2020**, *77*, 105505.
(60) Guo, L.; Zhu, X.; Sun, S.; Cong, C.; Zhou, Q.; Sun, X.; Liu, Y. Flexible semi-transparent organic transistors and circuits based on easily prepared polyphenyleneoxide dielectric. *Org. Electron.* **2019**, *69*, 308−312.
(61) Yi, M.; Shu, J.; Wang, Y.; Ling, H.; Song, C.; Li, W.; Xie, L.; Huang, W. The effect of porous structure of PMMA tunneling dielectric layer on the performance of nonvolatile floating-gate organic field-effect transistor memory devices. *Org. Electron.* **2016**, *33*, 95−101.
(62) Deman, A. L.; Tardy, J. PMMA-Ta2O5 bilayer gate dielectric for low operating voltage organic FETs. *Org. Electron.* **2005**, *6*, 78−84.
(63) Capelli, R.; Toffanin, S.; Generali, G.; Usta, H.; Facchetti, A.; Muccini, M. Organic light-emitting transistors with an efficiency that outperforms the equivalent light-emitting diodes. *Nat. Mater.* **2010**, *9*, 496−503.
(64) Jorgensen, W. L.; Maxwell, D. S.; Tirado-Rives, J. Development and testing of the OPLS all-atom force field on conformational energetics and properties of organic liquids. *J. Am. Chem. Soc.* **1996**, *118*, 11225−11236.
(65) Marcon, V.; Breiby, D. W.; Pisula, W.; Dahl, J.; Kirkpatrick, J.; Patwardhan, S.; Grozema, F.; Andrienko, D. Understanding structure-mobility relations for perylene tetracarboxydiimide derivatives. *J. Am. Chem. Soc.* **2009**, *131*, 11426−11432.


https://doi.org/10.1021/acs.jpcc.3c03332
J. Phys. Chem. C 2023, 127, 18026−18035

(66) Van Der Spoel, D.; Lindahl, E.; Hess, B.; Groenhof, G.; Mark, A. E.; Berendsen, H. J. GROMACS: Fast, flexible, and free. *J. Comput. Chem.* **2005**, *26*, 1701−1718.
(67) Lorenzoni, A.; Baldoni, M.; Besley, E.; Mercuri, F. Noncovalent passivation of supported phosphorene for device applications: From morphology to electronic properties. *Phys. Chem. Chem. Phys.* **2020**, *22*, 12482−12488.
(68) Nečas, D.; Klapetek, P. Gwyddion: An open-source software for SPM data analysis. *Cent. Eur. J. Phys.* **2012**, *10*, 181−188.
(69) Jeong, Y. J.; Jang, J.; Nam, S.; Kim, K.; Kim, L. H.; Park, S.; An, T. K.; Park, C. E. High-performance organic complementary inverters using monolayer graphene electrodes. *ACS Appl. Mater. Interfaces* **2014**, *6*, 6816−6824.
(70) Vasseur, K.; Rolin, C.; Vandezande, S.; Temst, K.; Froyen, L.; Heremans, P. A growth and morphology study of organic vapor phase deposited perylene diimide thin films for transistor applications. *J. Phys. Chem. C* **2010**, *114*, 2730−2737.
(71) Sun, B.; Xu, X.; Zhou, G.; Tao, L.; Xinran, W.; Chen, Z.; Xu, J.-B. Observation of Strong J-Aggregate Light Emission in Monolayer Molecular Crystal on Hexagonal Boron Nitride. *J. Phys. Chem. A* **2020**, *124*, 7340−7345.
(72) Xu, X.; Qiao, J.; Sun, B.; Tao, L.; Zhao, Y.; Qin, M.; Lu, X.; Ji, W.; Chen, Z.; Xu, J. Experimental Observation of Ultrahigh Mobility Anisotropy of Organic Semiconductors in the Two-Dimensional Limit. *ACS Appl. Electron. Mater.* **2020**, *2*, 2888−2894.



https://doi.org/10.1021/acs.jpcc.3c03332
*J. Phys. Chem. C* 2023, 127, 18026−18035